Editors' Suggestion

Turbulence Statistics of Arbitrary Moments of Wall-Bounded Shear Flows: A Symmetry Approach

Martin Oberlack,[1,2,*] Sergio Hoyas,[3] Stefanie V. Kraheberger,[1,2] Francisco Alcántara-Ávila,[3] and Jonathan Laux[1]
[1]Technical University of Darmstadt, Otto-Bernd-Straße 2, 64287 Darmstadt, Germany
[2]TU Darmstadt, Centre for Computational Engineering, Dolivostrasse 15, 64293 Darmstadt, Germany
[3]Instituto Universitario de Matemática Pura y Aplicada, UP València, Camino de Vera, 46024 València, Spain

(Received 19 May 2021; accepted 18 October 2021; published 10 January 2022)

The calculation of turbulence statistics is considered the key unsolved problem of fluid mechanics, i.e., precisely the computation of arbitrary statistical velocity moments from first principles alone. Using symmetry theory, we derive turbulent scaling laws for moments of arbitrary order in two regions of a turbulent channel flow. Besides the classical scaling symmetries of space and time, the key symmetries for the present work reflect the two well-known characteristics of turbulent flows: non-Gaussianity and intermittency. To validate the new scaling laws we made a new simulation at an unprecedented friction Reynolds number of 10 000, large enough to test the new scaling laws. Two key results appear as an application of symmetry theory, which allowed us to generate symmetry invariant solutions for arbitrary orders of moments for the underlying infinite set of moment equations. First, we show that in the sense of the generalization of the deficit law all moments of the streamwise velocity in the channel center follow a power-law scaling, with exponents depending on the first and second moments alone. Second, we show that the logarithmic law of the mean streamwise velocity in wall-bounded flows is indeed a valid solution of the moment equations, and further, all higher moments in this region follow a power law, where the scaling exponent of the second moment determines all higher moments. With this we give a first complete mathematical framework for all moments in the log region, which was first discovered about 100 years ago.

DOI: 10.1103/PhysRevLett.128.024502

One of the most successful ideas to understand and model turbulence was to use a statistical approach to turbulent flows. However, Reynolds, had already recognized that a complete statistical description of turbulence always leads to an infinite sequence of equations. For a solution of these equations, the sequence must be terminated and an empirical closure needs to be introduced which fundamentally deteriorates the prediction quality.

In addition to this fundamental difficulty, early turbulence researchers discovered that for canonical flows a universal behavior can be observed for the statistical moments. These universal regions of applicability are called turbulent scaling laws, and in this context, the logarithmic law of the wall was first postulated by von Kármán [1]. This, however, remained without any connection to the Navier-Stokes equations or any use of "first principles." In the decades that followed, there were several modifications of the log law (see, e.g., Ref. [2]), which also lacked any reference to the Navier-Stokes equations.

On the other hand, the idea that turbulent scaling laws are similarity solutions of statistical equations was probably first proposed by von Kármán and Howarth [3] for the decay of isotropic turbulence, and over time applied to innumerable flows. Maybe the first explicit use of symmetries in turbulence is due to Oberlack [4] to generate invariant solutions, which are synonymous with turbulent scaling laws but are solutions of statistical equations. Further work followed [5–7] even for complex flows with rotation, wall transpiration, and many more. All these approaches were limited to low order moments.

A central element of all these scaling laws was statistical symmetries. They were first detected in Ref. [8] in the infinite sequence of the multipoint moment equations (MPME). Further, in Ref. [9] it was shown that these symmetries are a measure of intermittency and non-Gaussian behavior of turbulence—both of which illustrate well-known, central characteristics of turbulent flows and which with the latter found a unique quantification in terms of symmetries.

The infinite sequence of the multipoint moment equations is formed from the Navier-Stokes equations,

$$\frac{\partial U_i}{\partial t} + U_k \frac{\partial U_i}{\partial x_k} + \frac{\partial P}{\partial x_i} - \nu \frac{\partial^2 U_i}{\partial x_k \partial x_k} = 0, \quad i = 1, 2, 3, \qquad (1)$$

$$\frac{\partial U_k}{\partial x_k} = 0, \tag{2}$$

where $t \in \mathbb{R}^+$, $x \in \mathbb{R}^3$, $\boldsymbol{U} = \boldsymbol{U}(\boldsymbol{x}, t)$, $P = P(x, t)$, and ν respectively represent time, position vector, instantaneous velocity vector, pressure, and kinematic viscosity. When dealing with statistical properties, typically, Reynolds's decomposition is used, i.e., $U_k = \bar{U}_k + u_k$, where $\overline{(\cdot)}$ denotes averaging and u_k is the turbulent fluctuations. We depart here from the usual approach to analyze moment equations based on the fluctuations and use instead statistical moments that are composed of the full instantaneous velocities. Based on this, generic multipoint velocity moments read

$$H_{i_{\{n\}}} = H_{i_{(1)}\ldots i_{(n)}} = \overline{U_{i_{(1)}}(\boldsymbol{x}_{(1)}, t) \cdots U_{i_{(n)}}(\boldsymbol{x}_{(n)}, t)}. \tag{3}$$

The moment hierarchy equation is derived by multiplying Eq. (1) by $n-1$ velocities at $n-1$ different locations $\boldsymbol{x}_{(i)}$ and performing a formal statistical averaging. The resulting MPME based on the instantaneous velocities for any order n reads

$$\frac{\partial H_{i_{\{n\}}}}{\partial t} + \sum_{l=1}^{n} \left(\frac{\partial H_{i_{\{n+1\}}[i_{(n)} \mapsto k_{(l)}]}[\boldsymbol{x}_{(n)} \mapsto \boldsymbol{x}_{(l)}]}{\partial x_{k_{(l)}}} + \frac{\partial I_{i_{\{n-1\}}[l]}}{\partial x_{i_{(l)}}} - \nu \frac{\partial^2 H_{i_{\{n\}}}}{\partial x_{k_{(l)}} \partial x_{k_{(l)}}} \right) = 0. \tag{4}$$

Here, $I_{i_{\{n-1\}}[l]}$ contains the pressure, while further details may be taken from Refs. [6,8].

The definitions (3) and the equations (4) are the basis of the symmetry theory. However, for the following comparison with the direct numerical simulation (DNS) data, we only consider one-point statistics; i.e., we apply $\boldsymbol{x} = \boldsymbol{x}_{(1)} = \boldsymbol{x}_{(2)} = \cdots = \boldsymbol{x}_{(n)}$ and, hence, the $H_{i_{\{n\}}}$ reduce to one-point moments. Further, as we presently limit ourselves to the moments of the streamwise velocity U_1, we subsequently only consider the nth moment $\overline{U_1^n}$.

The key property of the MPME for the following analysis is that (i) the system is linear and (ii) a coupling among moment equations exists only between the equations of order n and $n+1$. For a symmetry consideration, system (4) is considerably simpler but mathematically fully equivalent to the classical method based on Reynolds decomposition [8].

A symmetry refers to a variable transformation $\boldsymbol{x}^* = \boldsymbol{\phi}(\boldsymbol{x}, \boldsymbol{y}; a), \boldsymbol{y}^* = \boldsymbol{\psi}(\boldsymbol{x}, \boldsymbol{y}; a)$ which leaves a differential equation form invariant when it is written in the new $*$ variables, i.e., if the following holds:

$$\begin{aligned} &\boldsymbol{F}(\boldsymbol{x}, \boldsymbol{y}, \boldsymbol{y}^{(1)}, \boldsymbol{y}^{(2)}, \ldots, \boldsymbol{y}^{(p)}) = 0 \\ \Leftrightarrow\ &\boldsymbol{F}(\boldsymbol{x}^*, \boldsymbol{y}^*, \boldsymbol{y}^{*(1)}, \boldsymbol{y}^{*(2)}, \ldots, \boldsymbol{y}^{*(p)}) = 0, \end{aligned} \tag{5}$$

where $\boldsymbol{y}^{(p)}$ denotes the set of all pth derivatives of $\boldsymbol{y}$.

We focus here on the two scaling symmetries admitted by the Navier-Stokes equations in the limit of vanishing viscosity, which read

$$\begin{aligned} &T_{Sx/St}\colon\ t^* = e^{a_{St}} t, \qquad \boldsymbol{x}^* = e^{a_{Sx}} \boldsymbol{x}, \\ &\boldsymbol{U}^* = e^{a_{Sx} - a_{St}} \boldsymbol{U}, \qquad P^* = e^{2(a_{Sx} - a_{St})} P, \end{aligned} \tag{6}$$

which for the moments transform to

$$\begin{aligned} &\bar{T}_{Sx/St}\colon\ t^* = e^{a_{St}} t, \qquad \boldsymbol{x}^*_{(i)} = e^{a_{Sx}} \boldsymbol{x}_{(i)}, \\ &\overline{\boldsymbol{U}}^* = e^{a_{Sx} - a_{St}} \overline{\boldsymbol{U}}^*, \qquad \mathbf{H}^*_{\{n\}} = e^{n(a_{Sx} - a_{St})} \mathbf{H}_{\{n\}}. \end{aligned} \tag{7}$$

Once Eqs. (7) are implemented into Eq. (4), the scaling factors cancel, and they are indeed a symmetry transformation.

Note that viscosity is symmetry breaking, because unlike the Euler equation, which possesses two scaling symmetries, the Navier-Stokes equation admits only one scaling symmetry. In turbulence, however, viscosity acts only on the smallest scales with a length dimension of the order of Kolmogorov length. This fact is the basis of a multiscale expansion in the correlation space $\boldsymbol{r}$ in Ref. [10], in which it was shown that the velocity moments in the limiting case $\nu \to 0$ possess two scaling symmetries, i.e., in principle exactly like the Euler equation.

Besides these classical mechanical symmetries, the key for the new scaling laws to be derived below is the statistical symmetries. These symmetries cannot be directly identified in the Navier-Stokes equations, but only in the statistical equations derived from them, such as Eq. (4), and they thus also describe purely statistical properties of turbulence. The first one is a translation symmetry in the moments,

$$\begin{aligned} &\bar{T}'_{\{n\}}\colon\ t^* = t, \qquad \boldsymbol{x}^*_{(i)} = \boldsymbol{x}_{(i)}, \\ &\overline{\boldsymbol{U}}^* = \overline{\boldsymbol{U}} + \boldsymbol{a}, \qquad \mathbf{H}^*_{\{n\}} = \mathbf{H}_{\{n\}} + \mathbf{a}^H_{\{n\}}, \end{aligned} \tag{8}$$

which corresponds to non-Gaussianity (see Ref. [9]) while the statistical scaling symmetry,

$$\begin{aligned} &\bar{T}'_s\colon\ t^* = t, \qquad \boldsymbol{x}^*_{(i)} = \boldsymbol{x}_{(i)}, \\ &\overline{\boldsymbol{U}}^* = e^{a_{Ss}} \overline{\boldsymbol{U}}, \qquad \mathbf{H}^*_{\{n\}} = e^{a_{Ss}} \mathbf{H}_{\{n\}}, \end{aligned} \tag{9}$$

is due to the linearity of moment Eq. (4) and is a measure of intermittency as has been proven in Ref. [9]. With this, invariant solutions can now be constructed from the aforementioned symmetries (see, e.g., Ref. [6] and the Supplemental Material [11]). The characteristic system for the invariant solution for every $\overline{U_1^n}$ reads

$$\frac{dx_2}{a_{Sx}x_2 + a_{x_2}} = \frac{d\bar{U}_1}{[(a_{Sx} - a_{St}) + a_{Ss}]\bar{U}_1 + a^H_{1_{\{1\}}}} = \cdots = \frac{d\overline{U_1^n}}{[n(a_{Sx} - a_{St}) + a_{Ss}]\overline{U_1^n} + a^H_{1_{\{n\}}}}, \tag{10}$$

where we want to recall a_{Sx}, a_{St}, and a_{Ss} are the parameters of the three-parameter scaling group. Combining the groups (7) and (9) and using the one-point limit, we obtain

$$\bar{T}_{\text{scale}}: \; x_2^* = e^{a_{Sx}}x_2, \qquad \bar{U}_1^* = e^{a_{Sx}-a_{St}+a_{Ss}}\bar{U}_1, \ldots, \quad \overline{U_1^n}^* = e^{n(a_{Sx}-a_{St})+a_{Ss}}\overline{U_1^n}. \tag{11}$$

For the integration of Eq. (10), there are two cases to be distinguished and their solutions correspond to the log and center region [12]. The key parameter for the log law is the wall shear stress velocity $u_\tau = \sqrt{\tau_w/\rho}$, where τ_w is the wall shear stress and ρ is the density. u_τ uniquely determines the only velocity scale in the problem. For a given specific value, this implies that a scaling of the mean velocities according to Eq. (11) with arbitrary a_{Sx}, a_{S_t}, and a_{Ss} is no longer feasible. Hence, in terms of symmetry theory, u_τ is symmetry breaking for the mean velocity and for the group parameters in Eq. (11) this implies $a_{Sx} - a_{St} + a_{Ss} = 0$. Using this during the integration of Eq. (10) we obtain

$$\bar{U}_1 = \frac{a_1}{a_{Sx}} \ln\left(x_2 + \frac{a_{x_2}}{a_{Sx}}\right) + \tilde{C}_1, \tag{12}$$

$$\overline{U_1^n} = \tilde{C}_n \left(x_2 + \frac{a_{x_2}}{a_{Sx}}\right)^{\omega(n-1)} - \frac{a^H_{1_{\{n\}}}}{(n-1)(a_{Sx} - a_{St})}, \quad \text{with} \quad \tilde{C}_n = e^{c_n(n-1)(a_{Sx}-a_{St})}, \tag{13}$$

where $\tilde{C}_1$ and c_n represent integration constants and $\omega = 1 - a_{St}/a_{Sx}$. The three central results here are that in the log region for the mean velocity (i) the moment $n = 1$ follows a logarithmic law, (ii) the moments $n > 1$ behave like a power law, and (iii) the exponents for all nth moments are determined by a single parameter which is the exponent ω for the second moment.

In the second case no *a priori* symmetry breaking scale is introduced into Eq. (10); i.e., the factors $(a_{Sx} - a_{St} + a_{Ss}), \ldots, n(a_{Sx} - a_{St}) + a_{Ss}$ are all assumed to be nonzero. This results in power laws for all moments n, including the first moment $n = 1$. After the integration we observe that the parameters a_{Sx}, a_{St}, and a_{Ss} only occur as ratios and hence only two free parameters exist. If the exponents for the first two moments, σ_1 and σ_2, are given, we arrive at

$$\overline{U_1^n} = \tilde{C}'_n \left(x_2 + \frac{a_{x_2}}{a_{Sx}}\right)^{n(\sigma_2-\sigma_1)+2\sigma_1-\sigma_2} - \frac{a^H_{1_{\{n\}}}}{n(a_{Sx} - a_{St}) + a_{Ss}}, \quad \text{with} \quad \tilde{C}'_n = e^{c'_n[n(a_{Sx}-a_{St})+a_{St}]}, \tag{14}$$

where all c'_n are again constants of integration, $\sigma_1 = 1 - a_{St}/a_{Sx} + a_{Ss}/a_{Sx}$, and $\sigma_2 = 2(1 - a_{St}/a_{Sx}) + a_{Ss}/a_{Sx}$. The latter exponents of the first two moments uniquely determine the exponent of all higher moments.

The scaling laws (12)–(14) are to be validated in the following using new DNS data of a plane turbulent channel flow, with a Reynolds number of $\text{Re}_\tau = 10^4$ using the code LISO. The grid has roughly 80×10^9 points and the simulation ran for 50 million CPU-hours on 2048 processors. The details of this simulation are given in Ref. [12]. To clearly delimit the log from the deficit region, in what follows y^+ stands for the wall-based variable used for the log region; i.e., $y^+ = 0$ defines the wall. In the log region Eqs. (12) and (13) variables are nondimensionalized using ν and u_τ, obtaining

$$\bar{U}_1^+ = \frac{1}{\kappa}\ln(y^+) + B, \tag{15}$$

$$\overline{U_1^n}^+ = C_n(y^+)^{\omega(n-1)} - B_n, \quad \text{for } n \geq 2, \tag{16}$$

$$C_n = \alpha e^{\beta n}, \qquad B_n = \tilde{\alpha} e^{\tilde{\beta} n}, \quad \text{for } n \geq 2, \tag{17}$$

where in κ, B, B_n, C_n, α, β, $\tilde{\alpha}$, and $\tilde{\beta}$ we have subsumed the various constants appearing in Eqs. (12) and (13) and $y^+ = y u_\tau/\nu$, $\overline{U_1^n}^+ = \overline{U_1^n}/u_\tau^n$. κ refers to the usual von Kármán constant. We have obtained $\kappa = 0.394$; see discussion and comparison with other simulations [13–15] in Ref. [12]. The shift in y^+ by a_{x_2} in Eqs. (12) and (13) has been set to zero, although there are works [16] that suggest a nonzero shift. However, the numerical value is small and thus is negligible for large y^+. Interestingly, the data below show that the c_n in Eq. (13) are independent of n, so C_n results in a simple exponential function in n. Actually, this also results for B_n, although the reason for this is unknown.

Figure 1(a) shows the first central result of the present work, which is the comparison between DNS data for the moments $n \geq 2$ and Eq. (16). A double logarithmic plotting has been adopted to make the power laws visible more clearly. The universal numerical value ω in Eq. (16) has been chosen to $\omega = 0.10$ to match the DNS data and gives the best fit for all higher moments up to $n = 6$.

The two key results in Fig. 1(a) are (i) a nearly perfect representation of the power law for all moments solely based on the single parameter ω and (ii) the validity of all moments in the log law's range of validity of $y^+ \simeq 400 \ldots 2500$.

From Fig. 1(a) one might get the impression that the power-law scaling of Eg. (16) continues beyond the domain $y^+ \simeq 400 \ldots 2500$; however, it does not, as can be shown with the definition of a power-law indicator function:

$$\Gamma_n = \frac{y^+}{\overline{U_1^n}^+ + B_n} \frac{d\overline{U_1^n}^+}{dy^+} = \omega(n-1). \tag{18}$$

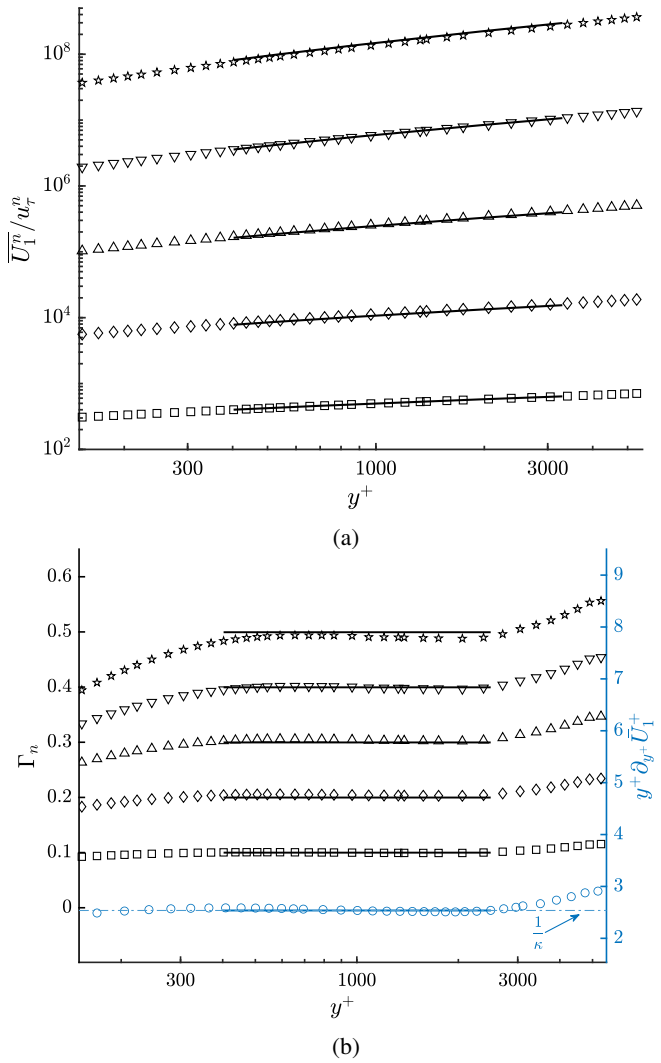

FIG. 1. Symbols $n = 1$ (circle); $n = 2$ (square); $n = 3$ (diamond); $n = 4$ (triangle); $n = 5$ (inverted triangle); $n = 6$ (star) DNS data. (a) Moments $\overline{U_1^n}^+$, solid line: Eq. (16) with coefficients fitted to DNS data for $n \geq 2$. (b) Left axis: Γ_n according to Eq. (18), solid line: $\Gamma_n = \omega(n-1)$ with $\omega = 0.10$ and $n \geq 2$. Right axis: log-indicator function $\Gamma = y^+\partial_{y^+}\tilde{U}_1^+ = \kappa^{-1}$ according to (15) with $\kappa = 0.394$.

DNS data are now inserted into Eq. (18) and compared with the exact value $\omega(n-1)$ in Fig. 1(b). It can be seen that especially for higher moments the constant range of validity stands out very clearly. The horizontal lines in Fig. 1(b) denote the theoretical values $\omega(n-1)$, and even for the highest moment with $n = 6$ the deviation is less than 2.1%. As the lowest line in Fig. 1(b) we have included the log-indicator function $\Gamma = y^+\partial_{y^+}\tilde{U}_1^+ = \kappa^{-1}$.

Further, it is important to verify the exponential scaling of C_n and B_n with n in Eq. (17) and an optimal agreement with the DNS data is shown in Fig. 2, where also the scaling of C_n' from Eq. (20) has been included. This scaling is due to the fact that the constants of integration c_n in Eq. (13)

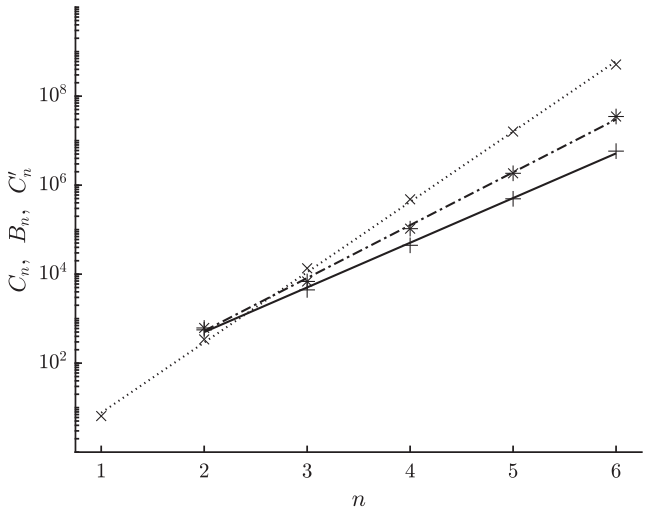

FIG. 2. Lines refer to coefficients C_n (solid line) and B_n (dash-dotted line) defined in Eq. (17) with $\alpha = 4.88$, $\beta = 2.31$, $\tilde{\alpha} = 2.23$, $\tilde{\beta} = 2.74$, and C_n' (dotted line) defined in Eq. (20) with $\alpha' = 0.21$, $\beta' = 3.64$; data points (+), (∗), and (×) are fitted directly to DNS data at $\mathrm{Re}_\tau = 10^4$.

emerging from Eq. (10) are independent of n and are all of order one. The deeper background for this is not fully evident so far.

In the center region of the channel the picture is quite different. To facilitate the discussion, the variable x_2 is used here for the deficit law, with origin $x_2 = 0$ on the channel center. A first symmetry-induced hint toward a power law in the form (14) in the center of a channel flow is found in Oberlack [4]. Therein, Oberlack formulated the mean velocity in the form of a deficit law, which is presently generalized for arbitrary moments of U_1. For this purpose, Eq. (14) is transformed accordingly and now has the universal deficit form,

$$\frac{\overline{U_1^n}^{(0)} - \overline{U_1^n}}{u_\tau^n} = C_n' \left(\frac{x_2}{h}\right)^{n(\sigma_2-\sigma_1)+2\sigma_1-\sigma_2}, \tag{19}$$

$$\text{with} \quad C_n' = \alpha' e^{\beta' n}, \tag{20}$$

and the exponent (0) in $\overline{U_1^n}^{(0)}$ refers to the values on the center line at $x_2 = 0$ and, similar to Eq. (17), α' and β' subsume various constants and are presumed to be universal.

In Fig. 3 all moments for the new DNS at $\mathrm{Re}_\tau = 10^4$ are shown in deficit form up to order $n = 6$. Even with the eye, it is visible that the curves have almost identical gradients, i.e., are largely independent of n. A curve fit of the data according to Eq. (19) reveals exactly this, namely that $\sigma_1 = 1.95$ and $\sigma_2 = 1.94$ have almost the same values. A comparison of the above exponents with the DNS data shows an extremely good approximation and the error in the exponents even for the highest moment $n = 6$ is far below 1%.

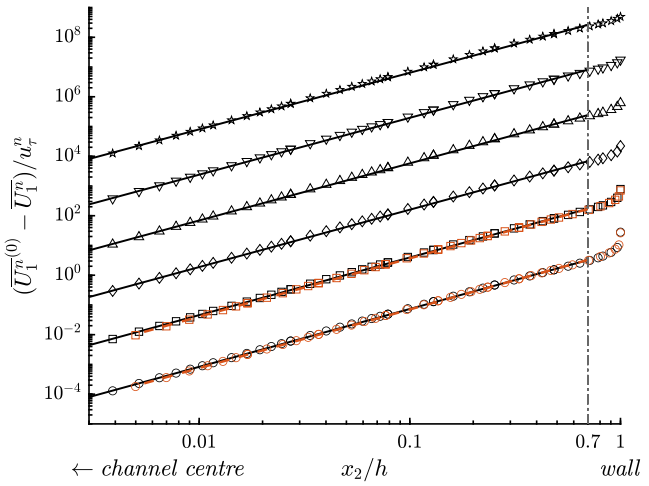

FIG. 3. Deficit scaling of $\overline{U_1^n}$ of order $n = 1, \ldots, 6$ in the channel center. Solid lines are according to Eq. (19). Symbols, DNS data as in Fig. 1. Red dashed lines and symbols, $\mathrm{Re}_\tau = 5200$ [15]. Vertical dot-dashed line, limit for the channel's center region defined by Eq. (19).

Compared to the log region, the deficit law is significantly less Reynolds number dependent. To demonstrate this, we have added DNS data at $\mathrm{Re}_\tau = 5200$ [15] for moments one and two. They collapse with the curves at $\mathrm{Re}_\tau = 10^4$. Also, the values for σ_1 and σ_2 are identical.

In both the log region (Fig. 1) and the deficit region (Fig. 3), it is visible that for the high moments, the functions take on high numerical values and this is significantly different than for moments formed on the fluctuations alone. At first, it appears that the logarithmic representation conceals errors for the high moments. In fact, this is not the case, as can be easily seen by dividing all the data by the corresponding C_n' in Fig. 3, for example. The curves are thereby only shifted vertically and the overall shape of each curve is preserved.

With $\sigma_1 \approx \sigma_2$ the exponent of the scaling law (19) is a constant and independent of the order n of the moments which is referred to as anomalous scaling. The constant exponent traces back to the statistical scaling symmetry a_{Ss} in Eq. (9) which is a measure for the intermittent behavior of turbulence. Hence statistical symmetries dominate in the center of the channel.

For practical applications two central conclusions can be drawn. First, the two scaling exponents for the first and second moments are sufficient to calculate the scaling of all higher moments. Specifically, these are for the log region κ and ω in Eqs. (15) and (16) and for the deficit law σ_1 and σ_2 in Eq. (19). Second, this also has central implications for turbulence model development. More precisely, the statistical symmetries developed in this work should be incorporated into turbulence models to make them reproduce the above-mentioned scaling laws [17].

Summarizing, we have shown how symmetry theory, one of the main tools of physics in the 20th century, can be used to overcome the problem related to the closure problem of turbulence. This has been possible due to the availability of a simulation at a Reynolds number large enough to clearly show the logarithmic layer and a generalized deficit law in the core region of the channel. Further research and finding of new statistical symmetries seem to be essential for the further development of this theory.

All data used in this paper can be downloaded from [18].

The authors gratefully acknowledge computing time on the Gauss Centre for Supercomputing e.V. on the GCS Supercomputer SuperMUC-NG at Leibniz Supercomputing Centre under Project No. pr92la, on the supercomputer Lichtenberg II at TU Darmstadt under Project No. project00072, and on the supercomputer CLAIX-2018 at RWTH-Aachen under Project No. bund0008. S. V. K. gratefully acknowledges funding from projects OB96/39-1 and M. O. for partial funding from OB 96/48-1, both financed by the German Research Foundation (DFG). S. H. and F. A.-A. were supported by Contract No. RTI2018-102256-B-I00 of Ministerio de Ciencia, innovación y Universidades/FEDER. F. A.-A. is partially funded by GVA/FEDER project ACIF2018. Finally, the authors thank Paul Hollmann for help with the manuscript.

*To whom correspondence should be addressed.
oberlack@fdy.tu-darmstadt.de

[1] T. von Kármán, Mechanische Ähnlichkeit und Turbulenz., Nachr. Ges. Wiss. Göttingen, Math.-Phys. Klasse 58 (1930).
[2] G. I. Barenblatt, Scaling laws for fully developed turbulent shear flows. Part 1. Basic hypotheses and analysis, J. Fluid Mech. **248**, 513 (1993).
[3] T. von Kármán and L. Howarth, On the statistical theory of isotropic turbulence, Proc. R. Soc. A **164**, 192 (1938).
[4] M. Oberlack, A unified approach for symmetries in plane parallel turbulent shear flows, J. Fluid Mech. **427**, 299 (2001).
[5] V. Avsarkisov, M. Oberlack, and S. Hoyas, New scaling laws for turbulent Poiseuille flow with wall transpiration, J. Fluid Mech. **746**, 99 (2014).
[6] M. Oberlack, M. Wacławczyk, A. Rosteck, and V. Avsarkisov, Symmetries and their importance for statistical turbulence theory, Mech. Eng. Rev. **2**, 15 (2015).
[7] H. Sadeghi and M. Oberlack, New scaling laws of passive scalar with a constant mean gradient in decaying isotropic turbulence, J. Fluid Mech. **899**, A10 (2020).
[8] M. Oberlack and A. Rosteck, New statistical symmetries of the multi-point equations and its importance for turbulent scaling laws, Discrete Continuous Dyn. Syst. **3**, 451 (2010).
[9] M. Wacławczyk, N. Staffolani, M. Oberlack, A. Rosteck, M. Wilczek, and R. Friedrich, Statistical symmetries of the Lundgren-Monin-Novikov hierarchy, Phys. Rev. E **90**, 013022 (2014).

[10] M. Oberlack and N. Peters, Closure of the two-point correlation equation in physical space as a basis for reynolds stress models, in *Near-Wall Turbulent Flows: Proceedings of the International Conference, Tempe, AZ, 1993*, edited by R. M. C. So and C. G. Speziale (Elsevier Science, New York, 1993), pp. 85–94.

[11] See Supplemental Material at http://link.aps.org/supplemental/10.1103/PhysRevLett.128.024502 for details on symmetry theory and deduction of Eqs. (11).

[12] S. Hoyas, M. Oberlack, F. Álcantara-Ávila, S. V. Kraheberger, and J. Laux, companion paper, Wall turbulence at high friction Reynolds numbers, Phys. Rev. Fluids **7**, 014602 (2021).

[13] S. Hoyas and J. Jiménez, Scaling of the velocity fluctuations in turbulent channels up to $Re_\tau = 2003$, Phys. Fluids **18**, 011702 (2006).

[14] M. Bernardini, S. Pirozzoli, and P. Orlandi, Velocity statistics in turbulent channel flow up to $Re_\tau = 4000$, J. Fluid Mech. **742**, 171 (2014).

[15] M. Lee and R. D. Moser, Direct numerical simulation of turbulent channel flow up to $\mathrm{Re}_\tau \approx 5200$, J. Fluid Mech. **774**, 395 (2015).

[16] B. Lindgren, J. M. Österlund, and A. V. Johansson, Evaluation of scaling laws derived from Lie group symmetry methods in zero-pressure-gradient turbulent boundary layers, J. Fluid Mech. **502**, 127 (2004).

[17] D. Klingenberg, D. Plümacher, and M. Oberlack, Symmetries and turbulence modeling, Phys. Fluids **32**, 025108 (2020).

[18] DNS data base of a turbulent channel flow at $\mathrm{Re}_\tau = 10000$, 10.48328/tudatalib-670.